the L-Pro[1] and L-Pro[2] residues enjoy true conformational freedom; these rings can flip from the major *N*-type conformation (in the $_{\beta}^{\gamma}T$-$^{\gamma}E$ region) into a minor *S* form (probably near to $_{\gamma}E$). This freedom is more pronounced in L-Pro[2] than it is in L-Pro[1]. Moreover, the flipping occurs in an independent fashion and not concerted. The D-Pro[3] residue appears to carry out large-amplitude oscillations inside a skewed well.

Matters appear more complicated in the case of (L[1]-0[2]-D[3]). The proposed existence[30] of two different twist-boat conformations of the nine-cycle is corroborated by the force-field minimizations. In each of the twist boats the two prolyl residues are predicted to enjoy some measure of conformational freedom, one of the flipping type, the other of the oscillating type. The coupling constant analysis leads to the conclusion that the two twist-boat froms cannot be present in nearly equal amounts but that one of them strongly predominates in solution. The predominant twist-boat resembles that found in the crystal.

Acknowledgment. We thank A. A. van Beuzekom for his assistance in the force-field calculations.

Registry No. *cyclo*(L-Pro$_3$), 2277-82-9; *cyclo*(L-Pro$_2$-L-Pro), 70493-40-2; *cyclo*(L-Pro-BzlGly-D-Pro), 85026-16-0.

Electrochemical Characterization of p-Type Semiconducting Tungsten Disulfide Photocathodes: Efficient Photoreduction Processes at Semiconductor/Liquid Electrolyte Interfaces

Joseph A. Baglio,*[1] Gary S. Calabrese,[2] D. Jed Harrison,[2] Emil Kamieniecki,[1] Antonio J. Ricco,[2] Mark S. Wrighton,*[2] and Glenn D. Zoski[1]

Contribution from the Department of Chemistry, Massachusetts Institute of Technology, Cambridge, Massachusetts 02139, and Advance Technology Laboratory, GTE Laboratories, Inc., Waltham, Massachusetts 02254. *Received August 23, 1982*

Abstract: Single-crystal p-type WS_2 ($E_g \approx 1.3$ eV) has been synthesized and characterized as an electrode material in CH_3CN/0.1 M $[n\text{-}Bu_4N]ClO_4$ and in aqueous electrolytes containing a variety of one-electron redox reagents having different $E_{1/2}$ values. In either CH_3CN or H_2O solvent the flat-band potential, E_{FB}, is measured to be $\sim$+0.95 V vs. SCE. In aqueous I_3^-/I^- the E_{FB} is shifted more negative by at least 0.3 V as is found for n-type WS_2 photoanodes. Capacitance measurements of the WS_2/electrolyte interface to determine E_{FB} accord well with electrochemical measurements. For $E_{1/2}$ more negative than E_{FB} the p-type WS_2 behaves as a photocathode giving an open-circuit photovoltage, E_V(oc), up to $\sim$0.8 V depending on $E_{1/2}$. For $E_{1/2}$ between +1.3 and −0.1 V vs. SCE, E_V(oc) varies as expected: for $E_{1/2}$ more positive than E_{FB} the p-type WS_2 behaves as a metallic electrode while for $E_{1/2}$ more negative than E_{FB} we find $E_V(oc) \approx |E_{1/2} - E_{FB}|$. It appears that for negative redox couples carrier inversion results at the p-WS_2 surface, but for $E_{1/2}$ more negative than −0.1 V vs. SCE E_V(oc) declines, a result associated with junction breakdown at sufficiently negative potentials. p-Type WS_2-based photoelectrochemical cells can be used to effect the sustained conversion of visible light (632.8 nm) to electricity in H_2O or CH_3CN with efficiencies of up to $\sim$7%. In H_2O the photochemical reduction to H_2 can be effected by illumination of p-type WS_2 modified by depositing $\sim 10^{-7}$ mol/cm^2 of Pd(0) or Pt(0) onto the surface as an H_2 evolution catalyst. Efficiency for H_2 evolution from 6 M H_2SO_4 is typically 6-7% for 632.8 nm (50 mW/cm^2) intensity.

There has been much interest in n-type semiconducting metal dichalcogenide, MY_2, electrodes for use in photoelectrochemical devices for conversion of light to electricity or chemical energy.[3-10] Efficient optical energy conversion has been realized with n-type MY_2 photoanodes, including a report of >10% efficiency for the

(1) GTE Laboatories, Inc.
(2) Massachusetts Institute of Technology.
(3) (a) Tributsch, H.; Bennett, J. C. *J. Electroanal. Chem.* **1977**, *81*, 97. (b) Tributsch, H. *Z. Naturforsch. A*, **1977**, *32A*, 972; *J. Electrochem. Soc.* **1978**, *125*, 1086; **1981**, *128*, 1261; *Ber. Bunsenges. Phys. Chem.*, **1977**, *81*, 361; **1978**, *82*, 169; *Sol. Energy Mater.* **1979**, *1*, 257; *Discuss. Faraday Soc.* **1980**, *70*, 189. (c) Gobrecht, J.; Tributsch, H.; Gerischer, H. *J. Electrochem. Soc.* **1978**, *125*, 2085; *Ber. Bunsenges. Phys. Chem.* **1978**, *82*, 1331. (d) Ahmed, S. M.; Gerischer, H. *Electrochim. Acta* **1979**, *24*, 705. (e) Kautek, W.; Gerischer, H.; Tributsch, H. *Ber. Bunsenges. Phys. Chem.* **1979**, *83*, 1000; *J. Electrochem. Soc.* **1980**, *127*, 2471. (f) Tributsch, H.; Gerischer, H.; Clemen, C.; Bucher, E. *Ibid.* **1979**, *83*, 655. (g) Kautek, W.; Gerischer, H. *Ber. Bunsenges. Phys. Chem.* **1980**, *84*, 645. (h) Kautek, W.; Gobrecht, J.; Gerischer, H. *Ibid.* **1980**, *84*, 1034. (i) Jaeger, C. D.; Gerischer, H.; Kautek, W. *Ibid.* **1982**, *86*, 20. (j) Clemen, C.; Saldana, X. I.; Muny, P.; Bucher, E. *Phys. Status Solidi A* **1978**, *49*, 437.
(4) (a) Lewerenz, H. J.; Heller, A.; DiSalvo, F. J. *J. Am. Chem. Soc.* **1980**, *102*, 1877. (b) Menezes, S.; DiSalvo, F. J.; Miller, B. *J. Electrochem. Soc.* **1980**, *127*, 1751. (c) Menezes, S.; Schneemeyer, L. F.; Lewerenz, H. J. *Appl. Phys. Lett.* **1981**, *38*, 949. (d) Lewerenz, H. J.; Ferris, S. D.; Doherty, C. J.; Leamy, H. J. *J. Electrochem. Soc.* **1982**, *129*, 418.
(5) (a) Fan, F.-R. F.; White, H. S.; Wheeler, B.; Bard, A. J. *J. Electrochem. Soc.* **1980**, *127*, 518. (b) Fan, F.-R. F.; White, H. S.; Wheeler, B. L.; Bard, A. J. *J. Am. Chem. Soc.* **1980**, *102*, 5142. (c) Abruna, H. D.; Bard, A. J. *J. Electrochem. Soc.* **1982**, *129*, 673. (d) White, H. S.; Abruna, H. D.; Bard, A. J. *Ibid.* **1982**, *129*, 265. (e) White, H. S.; Fan, F.-R. F.; Bard, A. J. *Ibid.* **1981**, *128*, 1045. (f) Nagasubrmanian, G.; Bard, A. J. *Ibid.* **1981**, *128*, 1055. (g) Frank, S. N.; Bard, A. J. *J. Am. Chem. Soc.* **1975**, *97*, 7427. (h) Laser, D.; Bard, A. J. *J. Am. Chem. Soc.* **1976**, *80*, 459.
(6) (a) Schneemeyer, L. F.; Wrighton, M. S. *J. Am. Chem. Soc.* **1979**, *101*, 6496; **1980**, *102*, 6964. (b) Schneemeyer, L. F.; Wrighton, M. S.; Stacy, A.; Sienko, m. J. *Appl. Phys. Lett.* **1980**, *36*, 701. (c) Kubiak, C. P.; Schneemeyer, L. F.; Wrighton, M. S. *J. Am. Chem. Soc.* **1980**, *102*, 6898. (d) Calabrese, G. S.; Wrighton, M. S. *Ibid.* **1981**, *103*, 6273.
(7) (a) Kline, G.; Kam, K.; Canfield, D.; Parkinson, B. A. *Sol. Energy Mater.* **1981**, *3*, 301. (b) Canfield, D.; Parkinson, B. A. *J. Am. Chem. Soc.* **1981**, *103*, 1249. (c) Furtak, T. E.; Canfield, D.; Parkinson, B. A. *J. Appl. Phys.* **1980**, *51*, 8018. (d) Parkinson, B. A.; Furtak, T. E.; Canfield D.; Kam, K.; Kline, G. *Discuss. Faraday Soc.* **1980**, *70*, 233.
(8) Baglio, J. A.; Calabrese, G. S.; Kamieniecki, E.; Kershaw, R.; Kubiak, C. P.; Ricco, A. J.; Wold, A.; Wrighton, M. S.; Zoski, G. D. *J. Electrochem. Soc.* **1982**, *129*, 1461.

0002-7863/83/1505-2246$01.50/0

conversion of solar energy to electricity.[7a] By way of contrast, relatively little has been published concerning the behavior of p-type MY_2 materials. p-Type WSe_2 is the only such material that has been examined in detail.[8-10] This material has been shown to give an open-circuit photovoltage of ~0.95 V that is quite encouraging.[10] Generally, relatively few p-type semiconductor photocathodes have proven to give efficient optical energy conversion in a photoelectrochemical device, compared to the number of n-type semiconductor photoanodes known to yield efficient conversion. The best p-type photoelectrode has been demonstrated to be p-type InP, band gap, E_g = 1.3 eV, that gives an open-circuit photovoltage of ~0.8 V.[11-13] p-Type Si, E_g = 1.1 eV, has also been studied extensively,[14-16] but yields less efficient photoreductions, owing to a lower open-circuit photovoltage of ~0.5 V. A number of other p-type semiconducting photocathodes have been characterized, including p-type GaAs, CdTe, and GaP, but relatively low efficiencies are obtained.[17-20] The excellent properties that we have found with synthetic n-type WS_2 photoanodes[6d,8] and the relative paucity of information on p-type MY_2 has prompted us to study the properties of p-type WS_2 as a photocathode.

An important issue relating to the interface energetics of semiconductor/liquid electrolyte junctions is the origin of an observed open-circuit photovoltage, E_V(oc), that is independent of the electrochemical potential, E_{redox}, of the contacting medium. For example, p-type InP appears to be "Fermi level pinned",[21] giving a photovoltage of 0.8 V for any E_{redox} more negative than ~−0.5 V vs. SCE.[12] The term Fermi level pinned means that the Fermi level at the surface of the semiconductor is pinned to a fixed position relative to the bottom of the conduction band, E_{CB}, and top of the valence band, E_{VB}. The Fermi level is pinned by a sufficient density and energetic distribution of surface states situated between E_{CB} and E_{VB},[21,22] as in the well-documented case of GaAs.[23] In the case of p-InP mentioned above the surface states[24] are just below the conduction band edge and the pinning gives rise to a good photovoltage[12] for couples that are sufficiently

Scheme I. (a) Interface Energetics for a Fermi Level Pinned p-Type Semiconductor Where the Barrier Height, E_B, Is the Difference between E_{VB} and E_{redox} and Is Fixed by Surface States. (b) Interface Energetics for a p-Type Semiconductor Having No Surface States between E_{VB} and E_{CB} and Where E_B Varies with E_{redox} in the "Ideal" Region of Potentials

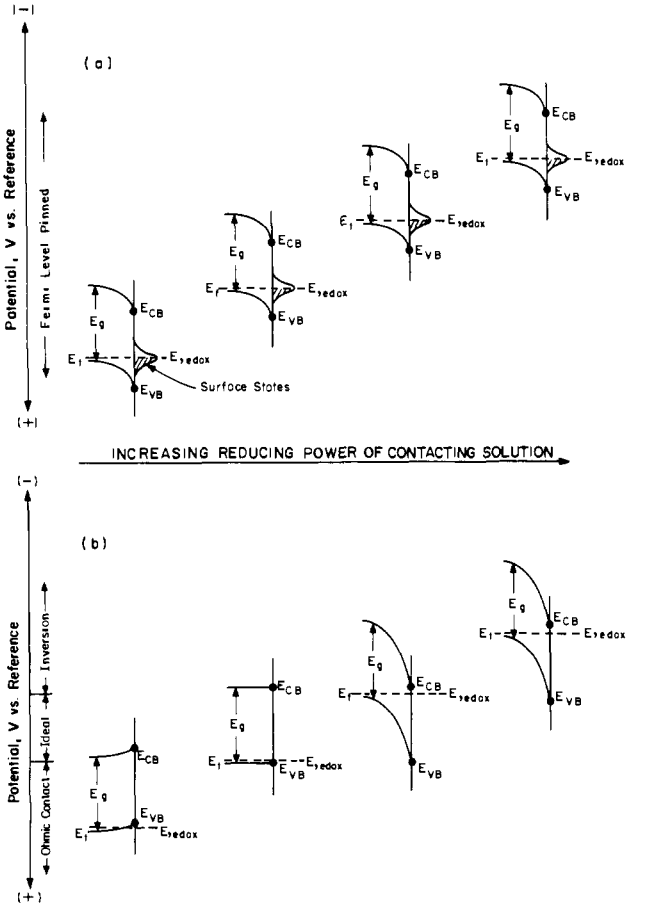

negative. When pinning occurs the barrier height, E_B, is independent of E_{redox} where E_B is approximately equal to E_V(oc) under high intensity, $\geq E_g$, illumination. Thus, interface diagrams as in Scheme Ia, as a function of E_{redox}, would correspond to a Fermi level pinned system.

Another rationale for an E_V(oc) that is independent of E_{redox} is so-called "carrier inversion".[25] When the value of E_B is greater than $0.5E_g$, the ratio of electrons to holes at the surface can be inverted compared to the bulk. When the semiconductor can be strongly inverted, the interface energetics could be represented by Scheme Ib. The inverted p-type semiconductor should behave as a buried p–n device with the solvent/electrolyte/E_{redox} combination providing the "ohmic contact" to the surface n-type layer. Consequently, the value of E_V(oc) should vary from zero for E_{redox} equal to, or positive of the flat-band potential $E_f = E_{FB}$, to E_V(oc) $\approx E_g$ for E_{redox} near E_{CB}. For E_{redox} more negative than E_{CB} the value of E_V(oc) would certainly be no more than E_g but could be less if the E_{redox} is so negative that dark current becomes significant owing to junction breakdown. It is likely that so-called MIS (metal/insulator/semiconductor) solar cells,[26] such as Si/SiO_2/metal, are examples of photovoltaic systems that behave according to Scheme Ib. The oxide must be of good enough quality and durability to remove interface states that might result in pinning, and yet the oxide must be thin to preclude a large series resistance. The distinction between pinning by surface states and inversion is not always clear. In the case of p-InP[12,24] the pinning is such that there is also a degree of inversion, but this depends

(9) (a) DeAngelis, L.; Scafe, E.; Galluzzi, F.; Fornarini, L.; Scrosati, B. *J. Electrochem. Soc.* **1982**, *129*, 1237. (b) Fornarini, L.; Stirpe, F.; Scrosati, B.; Razzini, G. *Sol. Energy Mater.* **1981**, *5*, 107. (c) Razzini, G.; Lazzari, M.; Bicelli, L. P.; Levy, F.; DeAngelis, L.; Galluzzi, F.; Scafe, E.; Fornarini, L.; Scrosati, B. *J. Power Sources* **1981**, *6*, 371. (d) Fornarini, L.; Stirpe, F.; Scrosati, B. *J. Electrochem. Soc.* **1982**, *129*, 1155.

(10) (a) Ginley, D. S.; Biefeld, R. M.; Parkinson, B. A.; Keung-Kam, K. *J. Electrochem. Soc.* **1982**, *129*, 145. (b) Ang, P. G. P.; Sammells, A. F. *Ibid.* **1982**, *129*, 233.

(11) Heller, A.; Miller, B.; Lewerenz, H. J.; Bachman, K. J. *J. Am. Chem. Soc.* **1980**, *102*, 6555.

(12) (a) Dominey, R. N.; Lewis, N. S.; Wrighton, M. S. *J. Am. Chem. Soc.* **1981**, *103*, 1261. (b) Dominey, R. N. Ph.D. Thesis, M.I.T., 1982.

(13) (a) Heller, A.; Vadimsky, R. G. *Phys. Rev. Lett.* **1981**, *46*, 1153. (b) Lewerenz, H. J.; Aspnes, D. E.; Miller, B.; Malm, D. L.; Heller, A. *J. Am. Chem. Soc.* **1982**, *104*, 3325.

(14) Bocarsly, A. B.; Bookbinder, D. C.; Dominey, R. N.; Lewis, N. S.; Wrighton, M. S. *J. Am. Chem. Soc.* **1980**, *102*, 3683.

(15) (a) Bruce, J. A.; Murahashi, T.; Wrighton, M. S. *J. Phys. Chem.* **1982**, *86*, 1552. (b) Dominey, R. N.; Lewis, N. S.; Bookbinder, D. C.; Bruce, J. A. *J. Am. Chem. Soc.* **1982**, *104*, 467. (c) Bookbinder, D. C.; Bruce, J. A.; Lewis, N. S.; Dominey, R. N. *Proc. Natl. Acad. Sci. U.S.A.* **1980**, *77*, 6280. Bruce, J. A.; Wrighton, M. S. *Isr. J. Chem.* **1982**, *22*, 184.

(16) Heller, A.; Lewerenz, H. J.; Miller, B. *J. Am. Chem. Soc.* **1981**, *103*, 200.

(17) Wrighton, M. S. *Acc. Chem. Res.* **1979**, *12*, 303.

(18) Tomkiewicz, M.; Fay, H. *Appl. Phys.* **1979**, *18*, 1.

(19) Harris, L. A.; Wilson, R. H. *Annu. Rev. Mater. Sci.* **1978**, *8*, 99.

(20) Nozik, A. J. *Annu. Rev. Phys. Chem.* **1978**, *29*, 189.

(21) Bard, A. J.; Bocarsly, A. B.; Fan, F.-R. F.; Walton, E. G.; Wrighton, M. S. *J. Am. Chem. Soc.* **1980**, *102*, 3671.

(22) (a) Lin, M.-S. Ph.D. Thesis, Harvard University, 1982. (b) Lin, M.-S.; Hung, N.; Wrighton, M. S. *J. Phys. Chem.*, to be submitted; *J. Electroanal. Chem.* **1982**, *135*, 121.

(23) (a) Spicer, W. E.; Lindau, I.; Skeath, P.; Su, C. Y.; Chye, P. *Phys. Rev. Lett.* **1980**, *44*, 420. (b) Kamieniecki, E.; Cooperman, G. *J. Vac. Sci. Technol.* **1981**, *19*, 453.

(24) (a) Spicer, W. E.; Gregory, P. E.; Chye, P. W.; Babalola, I. A.; Sikegawa, T. *Appl. Phys. Lett.* **1975**, *27*, 617. (b) Gudat, W.; Eastman, D. E.; Freeouf, J. L. *J. Vac. Sci. Technol.* **1976**, *13*, 250. (c) Spicer, W. E.; Lindau, I.; Pianetta, P.; Chye, P. W.; Garner, C. M. *Thin Solid Films* **1979**, *56*, 1. (d) Spicer, W. E.; Chye, P. W.; Garner, C. M.; Lindau, I.; Pianetta, P. *Surf. Sci.* **1979**, *86*, 763.

(25) Turner, J. A.; Manassen, J.; Nozik, A. J. *Appl. Phys. Lett.* **1980**, *37*, 488; *ACS Symp. Ser.* **1981**, *No. 146*, 253.

(26) Sze, S. M. "Physics of Semiconductor Devices", 2nd ed.; Wiley: New York, 1981; p 824.

on the position of the surface states. In GaAs[23] the surface states are distributed such that inversion on p-GaAs cannot occur. What is convincing about the InP case with respect to a role for surface states near the bottom of the conduction band is that the n-type InP gives a value of E_B no greater than ~500 mV,[12b,24] consistent with the larger barrier on p-type InP. If there were no surface states then the n-type InP would be expected to give a value of E_B similar to that for the p-type material.

It would appear that p-type WSe_2 (E_g(indirect) ≈ 1.2 eV[3e]) might be regarded as best fitting the representation in Scheme Ib, since the value of E_V(oc) = 0.95 V comes fairly close to E_g.[5] Further, the MY_2 materials appear to be relatively free of surface states that could cause pinning of the Fermi level.[27] However, it was previously concluded that surface states do play a role in n-type MoS_2- or $MoSe_2$-based systems. The main evidence was that E_V(oc) became independent of E_{redox} at a value where E_B was $<0.5E_g$ for MoS_2.[6a] The fixed E_V(oc) at a value significantly less than $0.5E_g$ seemingly rules out inversion. The ability to reduce the oxidized form of a redox couple in the dark at potentials positive of the most negative onsets for photoanodic current for the MoS_2 and $MoSe_2$ provides some evidence for surface states.[5g] For n-type WS_2 the maximun E_V(oc) in the E_{redox} independent region is ~0.7 V, not indicative of an E_B that causes strong inversion, though slightly larger than $0.5E_g$. For all of these cases we believe that the surface state density between E_{CB} and E_{VB}, while low, is sufficiently high[21] and its energetic distribution is such that it contributes to the fixed value of E_V(oc) as E_{redox} is varied. We now report a characterization of p-type WS_2 that appears, like p-WSe_2, to be relatively free of states between E_{CB} and E_{VB}. For the samples we have synthesized, E_{FB} = +0.95 V vs. SCE from determination of E_V(oc) vs. E_{redox} in H_2O/electrolyte or CH_3CN/electrolyte. These results are complemented by interface capacitance measurements[28] that give the same interface energetics deduced from the electrochemical measurements.

Experimental Section

Preparation of p-WS_2 Crystals and Electrode Preparation. The crystals of p-WS_2 were prepared by chlorine vapor transport of niobium-doped polycrystalline WS_2. The procedure is similar to that described previously for n-WS_2.[8] Further details of the preparation and electronic properties of these materials will be presented elsewhere. Flat, plate-like crystals of p-type WS_2 were peeled apart with fine tweezers to give paper-thin crystals, 0.01–0.1 cm^2 surface area, and were contacted with conducting silver epoxy and fashioned into electrodes as described earlier.[8] The surfaces of the electrodes were examined by microscopy and have been found to be similar to the morphology of n-WS_2 and are relatively free of surface defects and steps.

Electrochemical Procedures and Equipment for Cyclic Voltammetry and Current–Voltage Data. Cyclic voltammograms were recorded in Ar- or N_2-purged H_2O/0.1 M KCl and CH_3CN/0.1 M [n-Bu_4N]X, X = ClO_4, BF_4, solutions with redox reagents present at 1 mM by using a PAR Model 173 or ECO Model 551 potentiostat controlled by a PAR Model 175 programmer; scans were recorded with a Houston Instruments Model 2000 X-Y recorder. Except where otherwise stated, a single compartment, three-electrode cell was used with Pt counterelectrode and Ag/Ag^+ or saturated calomel (SCE) reference electrode for nonaqueous or aqueous media, respectively. The Ag/Ag^+ was +0.35 V vs. SCE in CH_3CN/0.1 M [n-Bu_4N]BF_4 or [n-Bu_4N]ClO_4. Measurements were made at 25 °C. Steady-state current voltage curves were recorded at low scan rates (≤20 mV/s) in well-stirred solutions under conditions of light intensity limited current.

Light sources included a 5 mW He–Ne laser (632.8 nm, 500:1 polarized; Aerotech Model LS5P) and a 5-W Ar ion laser (514.5 nm, Spectra Physics Model 164). Intensities were varied by using a beam expander and/or polarizing filter. A Tektronix J16 digital radiometer equipped with J6502 probe was used to measure intensities. Efficiency data are uncorrected for reflection losses or losses from electrolyte/redox couple/solution absorption.

Electroplating Pd(0) and Pt(0). The p-type WS_2 electrode was potentiostated between 0 and +0.1 V vs. SCE in an Ar- or N_2-purged 0.1 M KCl/1 mM K_2MCl_4/H_2O (M = Pd, Pt) solution and illuminated with ~50 mW/cm^2 of 632.8-nm light. Plating was discontinued after ~3 × 10^{-2} C/cm^2 had passed, as indicated by a PAR Model 179 digital coulometer.

Chemicals and Solvents. HPLC grade CH_3CN (Baker) was further dried and purified by distillation from P_2O_5; H_2O was distilled and deionized. Commercially available reagent grade electrolytes were used without further purification after confirming the absence of electroactive impurities over the potential range of interest; [n-Bu_4N]ClO_4 and [n-Bu_4N]BF_4 (Southwestern Analytical Co.) were dried in vacuo for more than 24 h at 70 and 40 °C, respectively.

Redox reagents, commercially available or synthesized and used in previous studies,[6] were used without additional purification provided the cyclic voltammetry at Pt revealed no electroactive impurities.

Auger Spectroscopy and Elemental Mapping. Auger spectra and elemental maps were obtained on a Physical Electronics Model 590 A scanning Auger spectrometer, utilizing a 5-keV electron beam at a current of 0.5–1 μA as excitation source and a cylindrical mirror analyzer for detection. Elemental signals were compared to literature values for identification.[29a] For sputtering (cleaning) the electrode surface, a differentially pumped ion gun provided a 2-keV Ar^+ beam. Elemental maps were recorded by rastering the focused (~1 μm) electron beam over the sample surface while monitoring the amplitude of the Auger peak for the desired element as a function of beam position on the surface; these data were recorded by using an oscilloscope equipped with a Polaroid camera.

For both Auger and XPS studies, electrodes were mounted as samples, after removal of the Pyrex tube, by fastening the copper wire to the sample holder, ensuring electrical grounding.

X-ray Photoelectron Spectroscopy. X-ray photoelectron spectra were obtained on a Physical Electronics Model 548 spectrometer equipped with Mg anode (Kα X-rays, $h\nu$ = 1254 eV) and cylindrical mirror analyzer. Pass energies were 100 eV for survey scans (0–1000 eV) and 25 or 50 eV for narrow scans (20-eV window about a specific elemental line). Elements were identified by comparison of observed core binding energies to literature values.[29b]

Photoacoustic Spectroscopy and Photoaction Spectra. The photoacoustic spectra of p-type WS_2 crystals (from one of the batches used for preparation of photocathodes) were recorded on a PAR Model 6001 photoacoustic spectrometer. Photoaction spectra were obtained by interfacing the photoacoustic spectrometer with a potentiostat.[8] The photoaction spectrum was recorded in 10 mM chloranil/0.1 M [n-Bu_4N]BF_4/CH_3CN at 25 °C with the photocathode poised at +0.2 V vs. Ag/Ag^+; the spectrum is not corrected for absorption by chloranil or [chloranil]$^-$.

Space-Charge Capacitance of p-WS_2. The surface photovoltage measured capacitance (SPMC) technique[28] was used to measure the space-charge capacitance of p-WS_2 as a function of potential in dry, deoxygenated CH_3CN/0.1 M [n-Bu_4N]ClO_4 but with no deliberately added redox reagents. The electrode potential was varied by using a potentiostat with a Pt counterelectrode and a Ag/Ag^+ reference electrode. The illumination was provided by a He–Ne laser (632.8 nm) attenuated with neutral density filters to an intensity of ~0.1 μW/cm^2. The incident 632.8-nm light was chopped at a frequency of 2 kHz. The capacitance data are independent of the frequency in the range 100 Hz to 10 kHz. The SPMC signal was detected with a high impedance source follower and a PAR Model 124A lock-in amplifier.

Results and Discussion

a. Spectral Response of p-Type WS_2. Like n-WS_2,[8] the photoacoustic and photoaction spectra of p-WS_2 onset at ~930 nm (1.3 eV), consistent with the known value of the indirect gap of n-WS_2.[8] Despite the 1.3-eV onset in the photoacoustic spectrum, the signal does not reach its limiting value until ~700 nm (1.8 eV), corresponding to the "direct gap" reported for n-WS_2.[8] The photoacoustic spectra of WS_2 are consistent with previously published optical properties of WS_2. In the photoaction spectrum in the onset region a plot of (relative $\Phi_e \times h\nu)^{1/2}$ vs. $h\nu$ is linear and should yield the indirect gap as the intercept on the $h\nu$ axis,[31]

(27) (a) Kama, A.; Enari, R. *Conf. Ser.-Inst. Phys.* **1979**, *No. 43*, Chapter 5. (b) McMenamin, J. C.; Spicer, W. E. *Phys. Rev. B: Condens. Matter* **1977**, *16*, 5474.

(28) Kamieniecki, E. *J. Vac. Sci. Technol.* **1982**, *20*, 811.

(29) (a) Davis, L. E.; MacDonald, N. C.; Palmberg, P. W.; Riach, G. E.; Weber, R. G. "Handbook of Auger Electron Spectroscopy", 2nd ed. Perkin-Elmer Corp.: Eden Prairie, MN, 1972; (b) Wagner, C. D.; Riggs, W. M.; Davis, L. E.; Moulder, J. F.; Muilenberg, G. E. "Handbook of X-Ray Photoelectron Spectroscopy"; Perkin-Elmer Corp.: Eden Prairie, MN, 1979.

(30) (a) Wilson, J. A.; Yoffe, A. D. *Adv. Phys.* **1969**, *18*, 193. (b) Tributsch, H. *Discuss. Faraday Soc.* **1980**, *70*, 189.

(31) (a) Butler, M. A. *J. Appl. Phys.* **1974**, *48*, 1914. (b) Johnson, E. J. In "Semiconductors and Semimetals"; Willardson, R. K., Beer, A. C., Eds.; Academic Press: New York, Vol. 3, Chapter 6. (c) Pankove, J. I. "Optical Processes In Semiconductors"; Dover Publications: New York, 1971; pp 35–61.

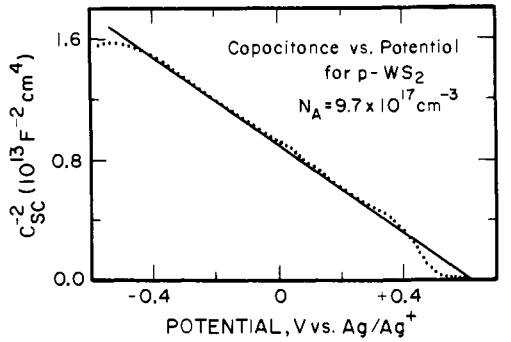

Figure 1. Mott–Schottky plot for p-WS_2 in contact with CH_3CN/0.1 M [n-Bu_4N]ClO_4. Data determined by the technique described in ref 28.

where Φ_e is the quantum yield for electron flow and $h\nu$ is the light energy. This procedure gives an indirect gap for p-WS_2 of 1.31 ± 0.05 eV. A plot of (relative $\Phi_e \times h\nu)^2$ vs. $h\nu$ is also linear and the intercept on the $h\nu$ axis gives the "direct" gap.[31] We find a direct gap for p-WS_2 of 1.80 ± 0.03 V. The indirect and direct gap for p-WS_2 are, within the uncertainties given, the same as found[8] for n-WS_2, as expected. For all photoelectrochemical experiments to be described below we have used either 632.8 or 514.5 nm light where the value of Φ_e should be maximum.

b. Capacitance vs. Potential for p-WS_2/CH_3CN/0.1 M [n-Bu_4N]ClO_4 Interfaces. The capacitance as a function of the electrode potential was measured by using the surface photovoltage measured capacitance (SPMC) technique.[28] This method permits the space-charge capacitance to be determined from the changes of the surface potential barrier induced by chopped light of photon energy exceeding the bandgap of the semiconductor. At low intensity and a high modulation frequency of the incident light, the measured SPMC signal is proportional to the reciprocal of the semiconductor surface space-charge capacitance, C_{sc}. The proportionality factor is entirely determined by the modulation frequency of the light, incident photon flux, and the reflection coefficient of the semiconductor.[28]

Figure 1 shows a typical plot of C_{sc}^{-2} vs. WS_2 electrode potential (Mott–Schottky plot) determined as outlined in the Experimental Section. In the depletion region, when C_{sc}^{-2} is proportional to the electrode potential, the slope of this Mott–Schottky plot gives the doping concentration in the space-charge region.[26,32] In estimating the doping concentration of WS_2, a value of 10 for the dielectric constant has been used.[33] The doping concentration for all measured samples was equal to about 1×10^{18} cm^{-3}. The value of the flat band potential, E_{FB}, was estimated by extrapolating the linear, depletion portion of the Mott–Schottky plot to the potential where $C_{sc}^{-2} = 0$. In all samples E_{FB} was found to be 0.60 ± 0.05 V vs. Ag/Ag^+ (+0.95 V vs. SCE), in good agreement with other electrochemical results reported in this paper (vide infra). At negative electrode potentials (≤−0.4 V vs. Ag/Ag^+) saturation of the space-charge capacitance was observed. The maximum band bending, E_{BB}, estimated from the saturation value of the C_{sc}^{-2}, was equal to 1.05 ± 0.05 V for all measured samples (for the sample of Figure 1, E_{BB} = 1.07 V). Since this value is close to the band gap of WS_2, 1.3 eV,[8] it seems probable that the saturation of C_{sc} is associated with the formation of an inversion layer at the surface of WS_2. It should be noted that, as determined by measuring the increase in phase shift of the SPMC signal,[34] the recombination rate of carriers increases at negative electrode potentials.

c. Behavior of Fast, One-Electron Redox Couples at p-Type WS_2 Compared to Behavior at Pt. As we[6,8] and others[5] have done previously, we have "mapped" the interface energetics of p-type WS_2 semiconductor photoelectrodes in solvent/electrolyte/redox couple systems where the couple is varied to alter E_{redox}. Such data complement the capacitance/potential results (Figure 1). A variety of redox couples, having different molecular structure and spanning a wide range of potential, has been examined at p-WS_2 in CH_3CN and H_2O. The data are summarized in Tables I and II and Figures 2–6. We will first consider the behavior of redox couples in CH_3CN/0.1 M [n-Bu_4N]ClO_4. Figure 2 shows a comparison of the cyclic voltammetry for three different redox couples at Pt and dark and illuminated p-WS_2. For the most positive redox couple, thianthrene, the cyclic voltammetry waves, in shape and position, are nearly the same at Pt and p-WS_2, independent of whether the p-WS_2 is illuminated. For the more

Table I. Comparison of p-WS_2 with Pt by Cyclic Voltammetry (100 mV/s) in CH_3CN/0.1 M [n-Bu_4N]ClO_4 Solutions

redox couple[a] (no.)	$E_{1/2}$[b] at Pt (V vs. Ag/Ag^+)	E_V(oc),[c] mV
[thianthrene]$^{+/0}$	+0.90	0
[diacetylferrocene]$^{+/0}$	+0.53	0
[MPT]$^{+/0}$ (23)	+0.38	~25
[TMPD]$^{2+/+}$	+0.35	150
[TTF]$^{2+/+}$	+0.35	150
[acetylferrocene]$^{+/0}$ (1)	+0.31	120
[Fe(η^5-C_5H_5)(η^5-$C_5H_4CH_2N(CH_3)_3$]$^{2+/+}$	+0.24	280
[ferrocene]$^{+/0}$ (2)	+0.06	400
[TTF]$^{+/0}$	0.00	640
[TCNE]$^{0/-}$ (3)	−0.09	580
[TCNQ]$^{0/-}$ (4)	−0.12	620
[chloranil]$^{0/-}$ (5)	−0.28	760
[decamethylferrocene]$^{+/0}$ (6)	−0.44	800
[TCNQ]$^{-/2-}$ (7)	−0.68	760
[MV]$^{2+/+}$ (8)	−0.80	690
[chloranil]$^{-/2-}$ (9)	−1.08	660
[Ru(acac)$_3$]$^{0/-}$ (10)	−1.10	360
[MV]$^{+/0}$ (11)	−1.20	480
[BAQ]$^{0/-}$ (21)	−1.30	360
[Ru(2,2'-bp)$_3$]$^{2+/+}$ (12)	−1.68	280
[Ru(2,2'-bp)$_3$]$^{+/0}$ (13)	−1.86	280
[BAQ]$^{-/2-}$ (22)	−1.96	330
[Ru(2,2'-bp)$_3$]$^{0/-}$ (14)	−2.10	280

[a] All data are for CH_3CN/0.1 M [n-Bu_4N]ClO_4 solutions at 25 °C, 100 mV/s. Redox couple concentrations are 1–5 mM. Numbers are keyed to Figure 5. MV is N,N'-dimethyl-4,4'-bipyridinium; TCNQ is tetracyanoquinodimethane; TCNE is tetracyanoethylene; MPT is 10-methylphenothiazine; TMPD is N,N,N',N'-tetramethyl-p-phenylenediamine; acac is acetylacetonate; TTF is tetrathiafulvene; BAQ is 2-*tert*-butyl-9,10-anthraquinone. [b] $E_{1/2}$'s were calculated from cyclic voltammetric data according to $E_{1/2} = (E_{PA} + E_{PC})/2$, where E_{PA}, E_{PC} are the anodic and cathodic current peaks, respectively. [c] $E_V(oc) = |E_{PC,Pt} - E_{PC,illum,p\text{-}WS_2}|$. Illumination was provided by a He-Ne laser (632.8 nm) at ~40 mW/cm².

Table II. Photovoltages from Pd-Treated p-WS_2 from Cyclic Voltammetry in H_2O/0.1 M KCl Solution

redox couple[a] (no.)	$E_{1/2}$[b] at Pt (V vs. SCE)	E_V(oc),[c] mV (Pd treated)[d]
[$IrCl_6$]$^{2-/3-}$ (15)	+0.670	150
[$Mo(CN)_8$]$^{3-/4-}$ (16)	+0.545	230
[Fe(η^5-C_5H_5)(η^5-$C_5H_4CH_2N(CH_3)_3$)]$^{2+/+}$ (17)	+0.370	310
[$Fe(CN)_6$]$^{3-/4-}$ (18)	+0.185	550
[$Ru(NH_3)_6$]$^{3+/2+}$ (19)	−0.185	750
[Ru(acac)$_3$]$^{0/-}$ (24)	−0.525	670
[MV]$^{2+/+}$ (20)	−0.665	520

[a] Data are for H_2O/0.1 M KCl solutions at 25 °C, 100 mV/s. Redox couple concentrations are 10 mM, except Ru(acac)$_3$ (2 mM). Numbers are keyed to Figure 5. [b] $E_{PA} + E_{PC})/2$, where E_{PA} and E_{PC} are anodic and cathodic current peaks, respectively. [c] $E_V(oc) = |E_{PC,Pt} - E_{PC,illum,p\text{-}WS_2}|$. Illumination was provided by a He-Ne laser (632.8 nm) at ~40 mW/cm². [d] Pd coverage corresponds to 3×10^{-2} C/cm² passed under illumination in a solution of K_2PdCl_4.

(32) Morrison, S. R. "Electrochemistry at Semiconductor and Oxidized Metal Electrodes"; Plenum Press: New York, 1980.
(33) Beal, A. R.; Liang, W. Y.; Hughes, H. P. *J. Phys. C* **1976**, *9*, 2449
(34) Kamieniecki, E., to be submitted.

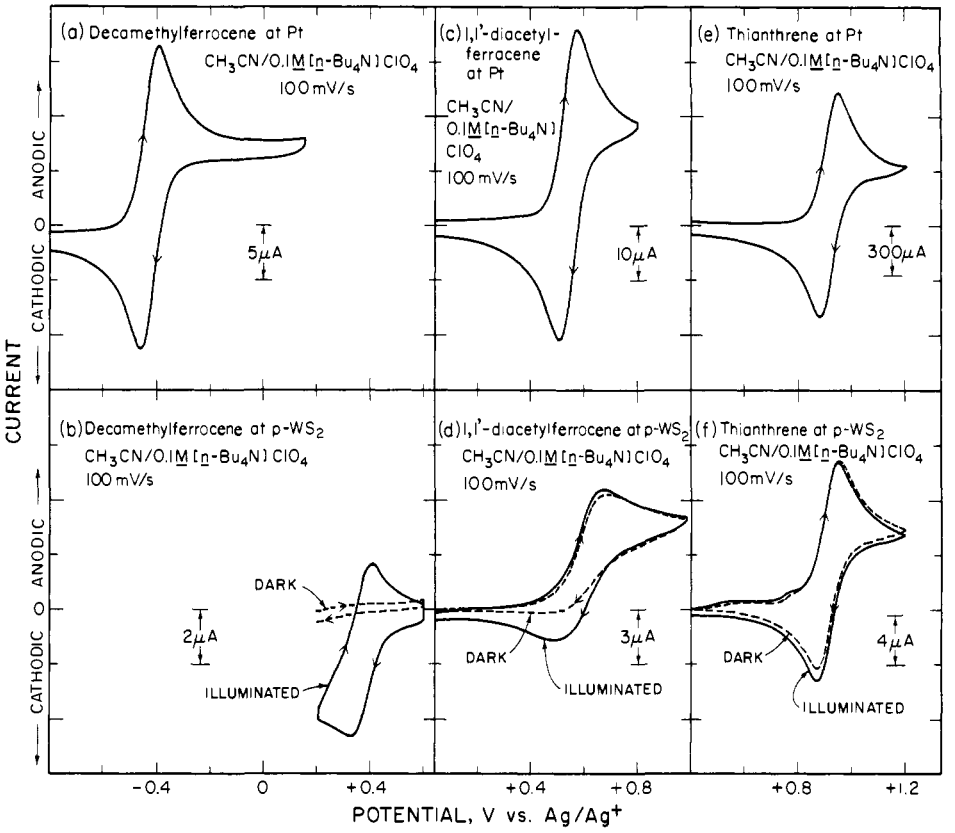

Figure 2. Comparison of the cyclic voltammetry of 1–5 mM solutions of various redox couples at Pt and p-WS_2. Illumination is at 632.8 nm.

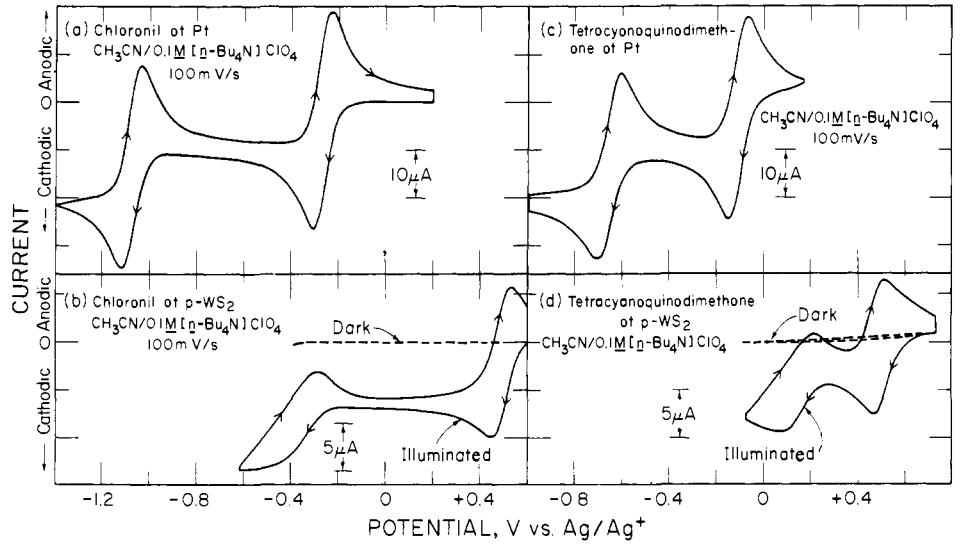

Figure 3. Cyclic voltammetry at Pt and p-WS_2 as in Figure 2 except that data are for chloranil and tetracyanoquinodimethane.

negative redox couples, however, there is a significant photoeffect associated with the p-WS_2 such that reduction of the oxidized form of the redox couple requires illumination of p-WS_2. For 1,1'-diacetylferrocene the photocathodic wave is at about the same position as the cathodic wave at Pt, but the photocathodic wave for the reduction of decamethylferricenium is ~0.8 V more positive than at Pt. The extent to which the cathodic peak is more positive at illuminated p-WS_2 is a measure of the extent to which the reduction process can be driven in an uphill sense. Thus, the ~0.8-V shift for the photocathodic reduction of decamethylferricenium is a measure of the open-circuit photovoltage, E_V(oc), and approximates the barrier height, E_B; cf. Scheme I. Actually, this technique to measure E_B underestimates the value by at least ~0.1 eV since there is an ~0.1-V difference between E_f and the top of the valence band. Further, E_V(oc) may be low for a variety of reasons including the use of a finite light intensity and nonideal interfacial electron transfer and recombination kinetics. Nonetheless, the cyclic voltammetry procedure gives a good relative measure of E_B and the position of the current peak, in contrast to the onset of current, is generally unequivocal both at Pt and at p-WS_2. Further, this procedure to measure E_V(oc) corresponds to a situation where both oxidized and reduced (roughly 1/1) forms of the redox couple are in contact with the electrode.

From the data in Figure 2 and the data in Figure 1 a good measure of consistency between the cyclic voltammetry and the capacitance is revealed. The Mott–Schottky plot, Figure 1, indicates that E_{FB} = +0.6 V vs. Ag/Ag^+ and therefore couples positive of this value should respond as they do at a metal. Thus, the thianthrene responds as at Pt and such a redox couple is regarded as contacting the valence band, forming an ohmic contact, Scheme Ib. As the $E_{1/2}$ of the couple is shifted more negative than +0.6 V vs. Ag/Ag^+ the value of E_B increases and

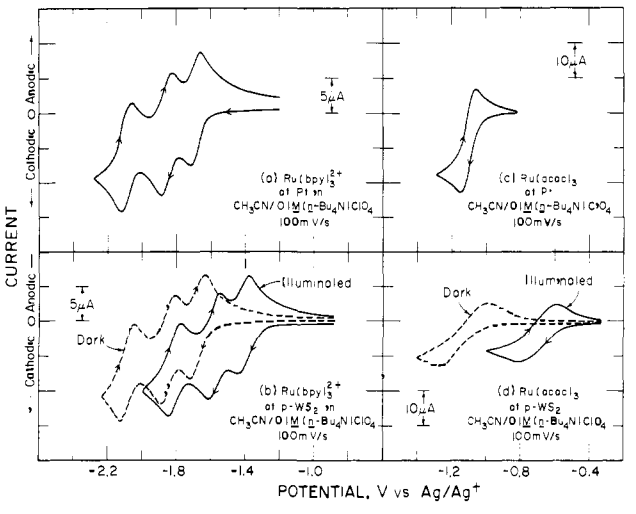

Figure 4. Cyclic voltammetry at Pt and p-WS_2 as in Figure 2 except that data are for $[Ru(2,2'\text{-bpy})_3]^{2+}$.

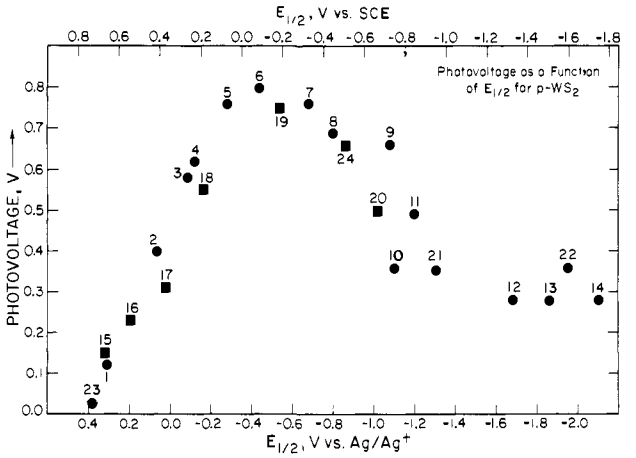

Figure 5. Plot of photovoltage against the $E_{1/2}$ value of the associated redox couple. Photovoltage is as defined in the text. The individual number entries are identified in Tables I and II for nonaqueous (●) and aqueous (■) media, respectively.

the shift in the photocathodic peak at p-WS_2 compared to the cathodic peak at Pt increases as shown by Figure 2.

The nearly ideal behavior reflected by the data in Figure 2 for three independently prepared solutions is substantiated by examination of the behavior of an CH_3CN/electrolyte solution containing 1 mM each of ferrocene ($E_{1/2}$ = +0.06 V vs. Ag/Ag$^+$), 1,2,3,4,5-pentamethylferrocene ($E_{1/2}$ = −0.19 V vs. Ag/Ag$^+$), and decamethylferrocene ($E_{1/2}$ = −0.44 V vs. Ag/Ag$^+$). At Pt, three one-electron waves are observed at the potential expected for the three redox couples. But at illuminated p-WS_2, one three-electron reduction process is observed with a current peak at ~+0.3 V vs. Ag/Ag$^+$ as would be expected for an ideal semiconductor. The key finding is that the photoreduction for all three one-electron reagents occurs at the same potential, consistent with the interfacial situation represented by Scheme Ib. The fact that onset of photocathodic current for couples between E_{CB} and E_{VB} is near the E_{FB} determined from the capacitance measurements is consistent with a surface that is relatively free of surface states.

For $E_{1/2}$ between ~+1.0 and −0.4 V vs. Ag/Ag$^+$ the p-WS_2/CH_3CN/electrolyte interface behaves ideally. For $E_{1/2}$ significantly more positive than ~+1.0 V vs. Ag/Ag$^+$, the p-WS_2 electrodes exhibit dark anodic corrosion processes that would be expected since holes are the majority charge carriers.[35] For $E_{1/2}$ more negative than ~−0.4 V vs. Ag/Ag$^+$, the consequences of carrier inversion at the p-WS_2 surface are revealed. This is most easily illustrated by considering redox couples that have two

(35) Bard, A. J.; Wrighton, M. S. *J. Electrochem. Soc.* **1977**, *124*, 1706.

Scheme II. Behavior of p-WS_2 in Contact with Redox Couple Having Different $E_{1/2}$ Values

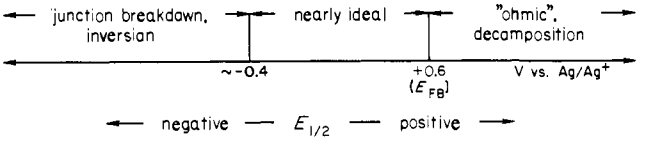

one-electron redox processes separated such that the first reduction occurs in the region where p-WS_2 behaves ideally and the second occurs more negative than −0.4 V vs. Ag/Ag$^+$, Figure 3. For both chloranil and TCNQ the reduction occurs in two one-electron processes at illuminated p-WS_2. Each of the one-electron reductions occurs at more positive potentials at illuminated p-WS_2 than at Pt but the extent to which each peak is shifted is about the same, 0.6–0.8 V. The carrier inversion results in a shift of the band edges of the semiconductor relative to E_{redox} such that the second reduction of TCNQ and chloranil can be effected. Thus, the value of E_B for the very negative redox couples does not increase beyond the ~0.8 V found for the decamethylferrocene couple. Indeed, for the second reduction of chloranil we see a somewhat smaller E_B than for the first reduction. The point here is that the photocathodic current peak for couples having $E_{1/2}$ more negative than ~−0.4 V vs. Ag/Ag$^+$ occurs at a different potential than for couples in the "ideal" regime. It appears that when E_{redox} is more negative than ~−0.4 V vs. Ag/Ag$^+$ the band bending, E_{BB}, is as large as possible and additional potential drop will occur across the Helmholtz layer, not across the semiconductor space-charge layer.

The behavior of *N,N'*-dimethyl-4,4'-bipyridinium, $[MV]^{2+}$, having two one-electron reductions negative of −0.4 V vs. Ag/Ag$^+$, is similar to that for chloranil. The reduction of $[MV]^{2+}$ to $[MV]^+$ and $[MV]^0$ occurs in two one-electron steps at electrode potentials that are more positive by ~0.5–0.8 V than at Pt. The cyclic voltammetric waves for the $[MV]^{2+/+/0}$ system at p-WS_2 are considerably broader than at Pt. Usually, the waves for all redox couples at p-WS_2 are somewhat broader than at Pt as the Figures show, but the waves for $[MV]^{2+/+/0}$ are especially broad. The relatively broad cyclic voltammetric waves for the $[MV]^{2+/+/0}$ system could be due to a relatively strong interaction with the p-WS_2 electrode. Perhaps surprisingly, flat molecules such as chloranil and TCNQ do not show any special interactions with the p-WS_2 electrode. Strong interactions might be expected based on the fact that the exposed surface of the WS_2 is a van der Waals plane not unlike that of graphite, which does have strong donor–acceptor interaction with such molecules.[36] The broad $[MV]^{2+/+/0}$ waves, though, are not unique. Typically, redox couples in the same potential regime behave similarly. We attribute the broad waves to the onset of the junction breakdown that ultimately gives reversible behavior in the dark when $E_{1/2}$ is sufficiently negative, Figure 4. Similar results have been reported earlier for p-type Si.[5h]

For $[Ru(2,2'\text{-bipyridine})_3]^{2+}$, the dark reduction voltammetric peak current varies linearly with (scan rate)$^{1/2}$ up to a scan rate of 1 V/s, indicating diffusion-controlled current. Due to the junction breakdown, the extent to which the reduction can be effected at a more positive electrode potential than at Pt is limited to ~300 mV. We can also correlate junction breakdown with the SPMC measurements, Figure 1, where the recombination rates are found to increase for negative electrode potentials.

Figure 5 summarizes the E_V(oc) vs. $E_{1/2}$ data collected in CH_3CN/electrolyte solutions with cyclic voltammetry, and Scheme II summarizes the behavior of the p-WS_2 based on these data. The behavior of p-WS_2 in aqueous electrolyte solutions has also been studied. However, it has proven to be quite difficult to obtain good cyclic voltammograms at p-WS_2 for redox couples that do respond well at Pt. Figure 6 illustrates some representative data. The p-WS_2 electrodes used all exhibit cyclic voltammograms for [chloranil]$^{0/-}$ in CH_3CN/0.1 M $[n\text{-}Bu_4N]ClO_4$ as represented

(36) Brown, A. P.; Koval, C.; Anson, F. C. *J. Electroanal. Chem.* **1976**, *72*, 379.

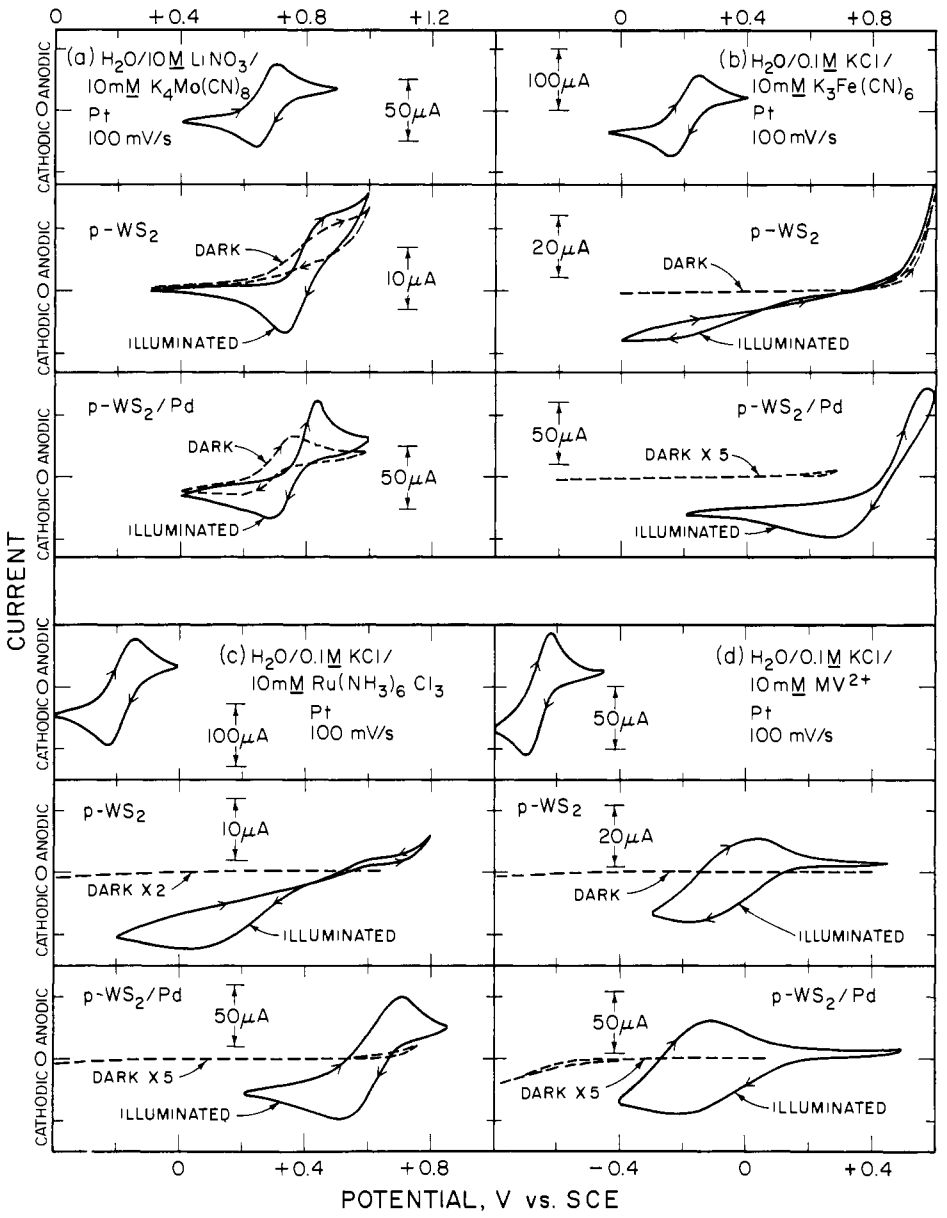

Figure 6. Comparison of cyclic voltammetry of various redox couples in aqueous solutions at Pt, p-WS_2 and Pd-treated p-WS_2. Illumination is at 632.8 nm (~40 mW/cm^2).

in Figure 3. For $[Ru(NH_3)_6]^{3+/2+}$ and $[Fe(CN)_6]^{3-/4-}$ the p-WS_2 electrodes give very poorly defined cyclic voltammograms, while $[Mo(CN)_8]^{3-/4-}$, which has a rather positive $E_{1/2}$, and $[MV]^{2+/+}$, which has a relatively negative $E_{1/2}$, give reasonably well-shaped cyclic voltammograms. For those cases where poorly defined waves are observed the deposition of a small amount of elemental Pd onto the p-WS_2 can significantly improve the appearance of the voltammogram, as illustrated in Figure 6 for $[Fe(CN)_6]^{3-/4-}$ and $[Ru(NH_3)_6]^{3+/2+}$. The electrodeposition of Pd onto the surface apparently does not form a p-WS_2/Pd Schottky barrier, since the photoeffects observed after the plating of Pd depend on $E_{1/2}$ of the redox couple. Similar results are obtained if Pt is electroplated instead, but the yield of well-behaved electrodes is lower (vide infra). If a Schottky barrier formed, E_V(oc) would be independent of $E_{1/2}$, since the photosensitive junction would be buried and act as a photovoltaic cell in series with the external circuit.[15b,37] The role of Pd or Pt is apparently to improve the overall interfacial electron-transfer kinetics for the reduction of $[Ru(NH_3)_6]^{3+/2+}$ and $[Fe(CN)_6]^{3-/4-}$. Table II summarizes E_V(oc) vs. $E_{1/2}$ data for Pd-treated p-WS_2 photocathodes in aqueous electrolytes and these entries are included in Figure 5. These results show that the interface energetics are essentially the same in the aqueous and nonaqueous media.

Improvement of the interfacial electron-transfer kinetics by plating Pd or Pt onto the p-WS_2 could be due to an improvement in the heterogeneous charge-transfer rate, to a reduction in surface recombination rates of electrons and holes, or to a combination of these two. With the data available it is not possible to unambiguously determine the relative importance of these factors. However, it seems reasonable to conclude that alteration of surface recombination by deposition of Pd or Pt is significant, since the heterogeneous electron transfer for species such as $[Ru(NH_3)_6]^{3+/2+}$ and $[Fe(CN)_6]^{3-/4-}$ is sufficiently fast that well-shaped cyclic voltammograms can generally be obtained at solid electrodes. Other workers have shown that surface recombination at semiconductor/liquid junctions can be diminished by metal deposition onto the semiconductor,[38] providing some precedence

(37) (a) Nakato, Y.; Abe, K.; Tsubomura, H. *Ber. Bunsenges. Phys. Chem.* **1976**, *80*, 1002. (b) Nakato, Y.; Tonomura, S.; Tsubomura, H. *Ibid.* **1976**, *80*, 1289.

(38) (a) Relson, R. J.; Williams, J. S.; Leamy, H. J.; Miller, B.; Heller, A. *Appl. Phys. Lett.* **1980**, *36*, 76. (b) Heller, A.; Lewerenz, H. J.; Miller, B. *Ber. Bunsenges. Phys. Chem.* **1980**, *84*, 592. (c) Parkinson, B. A.; Heller, A.; Miller, B. *Appl. Phys. Lett.* **1978**, *33*, 521; *J. Electrochem. Soc.* **1979**, *126*, 954.

for the conclusion here. It is conceivable, though, that the noble metal can improve the redox kinetics, since there may be a poor overlap of the appropriate states of the semiconductor and the solution redox species.[39] This possibility must be considered, since there is apparently a low density of surface states between E_{CB} and E_{VB} on p-WS_2 and the $[Ru(NH_3)_6]^{3+/2+}$ and $[Fe(CN)_6]^{3-/4-}$ systems are known to have relatively low self-exchange rates in aqueous solution. It is noteworthy that $[Mo(CN)_8]^{3-/4-}$, which has an $E_{1/2}$ near E_{VB}, and $[MV]^{2+/+}$, which has an $E_{1/2}$ near E_{CB}, give relatively good cyclic voltammograms at p-WS_2 without Pd treatment. This is consistent with good overlap between the energy levels of the redox couple and the appropriate p-WS_2 energy band. A strong point favoring the argument for improvement of the charge-transfer rate by metal deposition is the fact that the dark oxidation of $[Ru(NH_3)_6]^{2+}$ at p-WS_2, a process involving majority carriers and therefore unaffected by changes in recombination rate, is improved by plating Pd or Pt onto the p-WS_2. In H_2 evolution, vide infra, the Pd or Pt umambiguously catalyzes the interfacial redox process by improving H_2 evolution kinetics from the illuminated p-WS_2.

At this point the metal-treated p-WS_2 surface appears to be dominated by exposed WS_2 with respect to the energetics at the interface with the liquid electrolyte. That is, the Pd or Pt does not appear to uniformly cover the electrode to give a buried junction, Schottky or ohmic. Examination of Pd-treated p-WS_2 by scanning Auger elemental mapping spectroscopy shows rather uniform coverage of the Pd to the ~1-μm resolution possible. However, in both Auger and XPS, signals characteristic of WS_2 also appear, consistent with significant Pd-free areas on the WS_2 surface.[40] Thus, we conclude that the dominant role of Pd or Pt on the surface is to serve as a catalyst for interfacial electron transfer without altering the extent to which a reduction process can be driven uphill upon illumination of the WS_2.[41]

It is somewhat surprising that Pd and Pt can be useful as electron-transfer catalysts on p-WS_2, since the work functions of Pd and Pt would suggest that they could form ohmic contacts with p-WS_2, removing the barrier to dark reduction and causing the electrode to behave as a metal electrode. In fact, we do find that the metal deposition procedure does not always give good p-WS_2 electrodes: approximately 50% of the Pd-treated electrodes are "leaky", and even fewer of the Pt-treated surfaces result in satisfactory electrode performance, reflecting the formation of an ohmic contact over a fraction of the p-WS_2 surface. Attempts to deposit Au onto p-WS_2 always resulted in a significant fraction of the p-WS_2 being ohmic, and experiments could therefore not be done to determine whether Au would behave as Pd or Pt does to improve interfacial electron transfer.

The data for E_V(oc) vs. E_{redox} presented in Tables I and II and Figure 5 have been obtained from cyclic voltammetry, and we find the same energetics in CH_3CN and H_2O. The data accord well with the capacitance measurement, and further, the interface energetics for the samples of p-WS_2 are the same as previously reported[8] for n-WS_2, as would be expected. Measurements of E_V(oc) from p-WS_2 in aqueous solutions of variable pH (4–10) containing 1/1 $[Fe(CN)_6]^{3-}/[Fe(CN)_6]^{4-}$, E_{redox} = +0.22 V vs. SCE, have also been carried out in the conventional manner: the open-circuit potential difference between the illuminated p-WS_2 and a Pt gauze electrode was measured as a function of light intensity. At the highest light intensity the E_V(oc) measured was ~550 ± 50 mV independent of pH and in excellent agreement with the value expected from cyclic voltammetry measurements, Figure 5. The cyclic voltammetry of $[MV]^{2+/+}$ is likewise independent of pH. These data allow the conclusion that E_{FB} is independent of pH. Open-circuit photovoltage of p-WS_2 measured in the conventional manner has revealed one additional interesting finding: the value of E_V(oc) for I_3^-/I^- ($E_{1/2} \approx$ +0.30 V vs. SCE in H_2O electrolyte) shows a much smaller value (~0.2 V) than would be expected (~0.5 V) based on the curve in Figure 5. It is well-known that the I_3^-/I^- couple interacts strongly with n-WS_2[8] and other MY_2[3-7] semiconductors. For the p-WS_2 the E_{FB} apparently shifts more negative by at least 0.3 V leading to a smaller E_V(oc). This result illustrates one example of a strong interaction of the p-WS_2 with a redox species. None of the other redox substances investigated appear to affect E_{FB}.

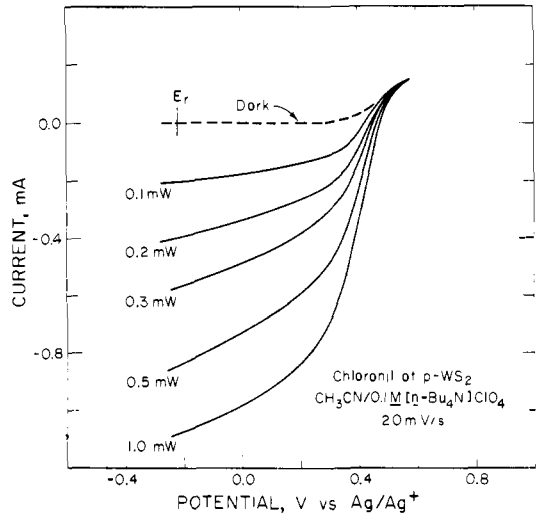

Figure 7. Steady-state photocurrent–voltage curves for a p-WS_2 electrode in CH_3CN/0.1 M $[n\text{-}Bu_4N]ClO_4$. Solution contained ~10 mM chloranil and a small amount of [chloranil]$^-$ such that E_{redox} = −0.22 V vs. Ag/Ag^+. Irradiation was provided at 632.8 nm. Data from these curves are given in Table III.

Steady-State Photoreduction at Illuminated p-WS_2 Electrodes. The wavelength dependence of the photocurrent for p-WS_2, showing strong visible response onsetting at ~900 nm, and the large E_V(oc), ~0.8 V, for redox couples with $E_{1/2}$ in the vicinity of −0.4 V vs. Ag/Ag^+, suggest that photoelectrochemical energy conversion processes based on p-WS_2 should be relatively efficient. Figure 7 shows steady-state photocurrent–voltage curves as a function of 632.8-nm light intensity for a p-WS_2-based cell for the [chloranil]$^{0/-}$ system poised to E_{redox} = −0.22 V vs. Ag/Ag^+ in CH_3CN/0.1 M $[n\text{-}Bu_4N]ClO_4$. In such curves key parameters include the open-circuit photovoltage, E_V(oc), the quantum yield for electron flow at E_{redox}, Φ_e, and the fill factor, FF.[8] From these curves the maximum efficiency for converting input optical energy to electricity, η_{max}, can be deduced. Output parameters associated with the curves in Figure 7 are given in Table III, which includes data from photocurrent–voltage curves in nonaqueous and aqueous media where the full cell chemistry can be represented by eq 1 and 2 for the photocathodic and counterelectrode processes, respectively. In such cases, the only output from the cell is electricity and no net chemical change occurs.

$$A^+ + e^- \rightarrow A \text{ (p-}WS_2\text{, photocathode)} \quad (1)$$

$$A \rightarrow A^+ + e^- \text{ (counterelectrode)} \quad (2)$$

Data for [chloranil]$^{0/-}$, [decamethylferrocene]$^{+/0}$, and $[Ru(NH_3)_6]^{3+/2+}$ are given since their E_{redox} values can be adjusted such that E_V(oc) is near the optimum of ~0.8 V (Figure 5). Values of E_V(oc) do agree well with photovoltage measurements from cyclic voltammetry. The values of Φ_e are up to ~0.6, uncorrected for reflection or solution absorption losses. Unfortunately, FF is typically below 0.5, leading to lower than expected efficiencies. Nonetheless, the values of η_{max} significantly exceed those routinely found for p-Si-based devices[14,15] studied in this laboratory under the same conditions. The efficiency for electricity

(39) (a) Reference 32; pp 101, 221. (b) Gerischer, H. In "Physical Chemistry: An Advanced Treatise"; Eyring, H., Henderson, D., Jost, W., Eds.; Academic Press: New York, 1970; Vol. 9A, Chapter 5.

(40) Other workers have found that thin metal films deposit onto semiconductors in the form of very small "islands": (a) Gerischer, H.; Lubke, M. *Z. Phys. Chem. (Wiesbaden)* **1975**, *98*, 317. (b) Goldstein, B.; Szostak, D. J. *J. Vac. Sci. Technol.* **1980**, *17*, 718. See also: Simon, R. A.; Ricco, A. J.; Harrison, D. J.; Wrighton, M. S. *J. Phys. Chem.*, in press.

(41) The phenomenon of noble metal catalyst deposition showing no effect on semiconductor/liquid junction interfacial energetics has precedence: see ref 37 and 15b.

Table III. Representative Output Parameters for p-WS_2-Based Photoelectrochemical Cells

electrolyte system[a]	input pwr, mW[b] (power density, mW/cm²)	Φ_e[c] at E_{redox}	E_V(oc), (E_V at η_{max}, mV)	η_{max},[e] %	fill factor[f]
CH_3CN/0.1 M [n-Bu_4N]ClO_4/10 mM [chloranil]$^{0/-}$, E_{redox} = −0.22 V vs. Ag/Ag^+ naked p-WS_2 (1)	0.10 (3.2)	0.40	640 (540)	5.4	0.42
	0.20 (6.4)	0.40	660 (540)	5.4	0.41
	0.30 (9.5)	0.37	660 (540)	5.0	0.41
	0.50 (15.9)	0.32	680 (520)	4.9	0.43
	1.00 (31.8)	0.21	700 (500)	2.5	0.52
CH_3CN/0.1 M [n-Bu_4]ClO_4/4 mM [decamethylferrocene]$^{+1/0}$, E_{redox} = −0.38 V vs. Ag/Ag^+ naked p-WS_2 (2)	0.025 (0.8)	0.38	730 (440)	7.0	0.48
	0.050 (1.6)	0.36	780 (440)	7.0	0.46
	0.100 (3.2)	0.38	810 (440)	7.0	0.44
	0.200 (6.4)	0.29	830 (440)	5.0	0.39
6 M H_2SO_4, $E^{\circ\prime}(H_2O/H_2)$ = −0.14 V vs. SCE Pt-treated p-WS_2 (3)	0.20 (6.4)	0.41	660 (380)	5.7	0.40
	0.50 (15.9)	0.38	700 (380)	5.8	0.40
	1.00 (31.8)	0.38	760 (380)	5.8	0.38
	1.30 (41.4)	0.38	780 (380)	5.7	0.39
	2.20 (70.0)	0.38	780 (380)	5.5	0.35
H_2O/0.1 M KCl/50 mM $Ru(NH_3)_6Cl_3$, E_{redox} = −0.104 V vs. SCE naked p-WS_2 (4)	0.064 (2.0)	0.58	680 (380)	7.4	0.37
	0.127 (4.0)	0.56	700 (380)	6.6	0.33
	0.250 (8.0)	0.54	720 (380)	6.4	0.32
H_2O/0.1 KCl/50 mM $Ru(NH_3)_6Cl_3$, E_{redox} = −0.070 V vs. SCE Pd treated p-WS_2 (4)	0.063 (2.0)	0.49	670 (370)	6.2	0.37
	0.127 (4.0)	0.50	700 (390)	6.4	0.37
	0.252 (8.0)	0.48	730 (410)	6.5	0.36
H_2O/0.1 M KCl/50 mM $Ru(NH_3)_6Cl_3$, E_{redox} = −0.104 V vs. SCE naked p-WS_2 (5)	0.063 (2.0)	0.56	640 (308)	5.1	0.28
	0.130 (4.1)	0.42	640 (260)	2.6	0.19
	0.256 (8.1)	0.41	680 (310)	3.4	0.24
H_2O/0.1 M KCl/50 mM $Ru(NH_3)_6Cl_3$, E_{redox} = −0.070 V vs. SCE Pd treated p-WS_2 (5)	0.063 (2.0)	0.53	700 (330)	6.8	0.36
	0.127 (4.0)	0.53	730 (370)	6.9	0.35
	0.253 (8.1)	0.52	750 (370)	6.5	0.33
	0.580 (18.5)	0.47	760 (310)	5.0	0.27

[a] Data for the chloranil and H_2 systems are from curves in Figures 9 and 10, respectively. Electrode numbers refer to independently prepared electrodes, the comparison of "naked" and Pd-treated is with the same p-WS_2 samples 4 and 5 examined under the same conditions. [b] Input power is at 632.8 nm. [c] Quantum yield for electron flow at E_{redox} (or $E^{\circ\prime}(H_2O/H_2)$). Data are ±15% and are uncorrected for reflection or solution absorption. [d] Photovoltages; E_V(oc) is the difference in onset of photocurrent and E_{redox}. E_V at η_{max} is the difference between the potential at the maximum power point and E_{redox}. [e] η_{max}, % is defined in ref 8. [f] Fill factor is defined in ref 8.

generation can be maintained for at least 100 h without decline. The values of η_{max} are typically ~7% from the best p-WS_2 electrodes for redox couples where E_{redox} is near −0.4 V vs. Ag/Ag^+. More positive redox couples, e.g., $[Fe(CN)_6]^{3-/4-}$, give smaller E_V(oc) and lower overall η_{max}. Further, more negative redox couples, e.g., $[MV]^{2+/+}$, give poor overall η_{max} owing to low FF or to a combination of low FF and low E_V(oc). The poor behavior for the negative redox couples is in accord with conclusions that the negative potentials can be associated with junction breakdown. The lower η_{max} for the positive redox couples follows expectation in that lower E_V(oc) would be expected as E_{redox} moves closer to E_{FB}.

Another point that the steady-state data reveal is that a good cyclic voltammogram at illuminated p-WS_2 does not necessarily signal good power conversion efficiency, as illustrated by the $[MV]^{2+/+}$ system in H_2O or CH_3CN where we have not been able to achieve >2% efficiency using electrodes that give >7% for redox couples such as $[Ru(NH_3)_6]^{3+/2+}$ in H_2O or [chloranil]$^{0/-}$ in CH_3CN. The Pd or Pt treatment of p-WS_2 does not improve the efficiency in the $[MV]^{2+/1+}$ case. Furthermore, a poor cyclic voltammogram does not necessarily signal poor steady-state output parameters, as the data for $[Ru(NH_3)_6]^{3+}$ show. These results are not inconsistent. Since the electron-transfer rate is presumably first order in concentration, the increased concentration of $[Ru(NH_3)_6]^{3+}$ allows better competition with electron-hole recombination. The relatively poor η_{max} from the $[MV]^{2+/+}$ cell is somewhat surprising but at least serves to underscore the importance of examining the steady-state parameters to fully ascertain the interfacial properties. The firm conclusions regarding photovoltage from cyclic voltammetry are substantiated fully by the steady-state data, but it should be emphasized that these results relate only to interface energetics, not kinetics.

The steady-state data for $[Ru(NH_3)_6]^{3+/2+}$ also show that the Pd treatment does not always yield improvement, whereas we do not find good cyclic voltammetry without Pd treatment. Generally, the Pd treatment can yield improvement when the naked electrode does not give the ~7% efficiency characteristic of the best electrodes. For good naked p-WS_2 electrodes (i.e., those giving an η_{max} of ~7%) the deposition of Pd onto the surface sometimes leads to a deterioration of efficiency (by reduction in Φ_e), but the decline is typically less than 10%. The improvement in output parameters upon Pd deposition when starting with a poor η_{max} from the naked electrode can be interpreted as due to increase in the electron-transfer rate so that competition with recombination is better. We do find p-WS_2 electrodes that give good η_{max} in the CH_3CN/0.1 M [n-Bu_4N]ClO_4/[chloranil]$^{0/-}$ system but give poor η_{max} in the H_2O/0.1 M KCl/$[Ru(NH_3)_6]^{3+/2+}$ system. This result seems to confirm a role for Pd in enhancing electron transfer for the $[Ru(NH_3)_6]^{3+/2+}$ reduction when the surface has a higher recombination velocity, since good p-WS_2 electrodes give ~7% efficiency with either the $[Ru(NH_3)_6]^{3+/2+}$ or the [chloranil]$^{0/-}$ system.

Hydrogen Generation from Illuminated p-WS_2 Photocathodes. Data for steady-state H_2 evolution from Pd-treated and Pt-treated p-WS_2 photocathodes are given in Table IV. As for the other small band gap p-type semiconductors, the naked surface of p-WS_2 is not a good one from which to evolve H_2. Proof for poor kinetics comes from experimentation with redox couples such as $[MV]^{2+/+}$ in H_2O which can be reduced, whereas H_2O is not reduced under the same conditions at a pH where $E^{\circ\prime}([MV]^{2+/+}) = E^{\circ\prime}(H_2O/H_2)$. The deposition of Pd or Pt onto the surface of the p-WS_2 results in a dramatic improvement in efficiency for H_2 generation, as shown in Figure 8. A similar finding has been reported for p-WSe_2[3h] and other p-type semiconductors.[13,15,37b]

Data in Tables III and IV give efficiency parameters for H_2 evolution, where η_{max} is given by eq 1 and E_V is the extent to which the p-WS_2 electrode potential is positive of $E^{\circ\prime}(H_2O/H_2)$. The E_V(oc) of ~0.8 V is not sufficiently great that light alone can be used to split H_2O into H_2 and O_2; that requires a minimum of 1.23 V. Thus, p-WS_2 photoelectrodes can be used to assist the

Table IV. Effect of pH on Output Parameters for Pd- or Pt-Treated p-WS_2 Photocathodes for H_2 Generation

aqueous electrolyte system[a]	input power,[b] mW (mW/cm²)	Φ_e[c] at E_{redox}	E_V(oc),[d] mV (E_V at η_{max}, mV)	η_{max},[e] %	fill factor[e]
		p-WS_2/Pt 6			
pH 7, phosphate	0.10 (5.7)	0.32	510 (150)	1.0	0.12
pH 5, acetate		0.47	640 (200)	2.6	0.17
pH 3, chloroacetate		0.48	720 (240)	3.9	0.22
0.5 M H_2SO_4		0.53	840 (370)	6.7	0.29
6 M H_2SO_4		0.50	720 (380)	7.4	0.40
		p-WS_2/Pt 7			
0.5 M H_2SO_4	0.064 (7.8)	0.45	860 (430)	7.0	0.35
3 M H_2SO_4		0.44	850 (450)	7.2	0.37
6 M H_2SO_4		0.44	750 (460)	7.6	0.45
9 M H_2SO_4		0.40	720 (380)	6.5	0.45
12 M H_2SO_4		0.41	510 (320)	4.0	0.37
		p-WS_2/Pd 8			
3 M H_2SO_4	0.082 (4.6)	0.67	750 (400)	9.8	0.38
6 M H_2SO_4		0.74	730 (480)	12.0	0.45
9 M H_2SO_4		0.62	600 (360)	7.9	0.42
12 M H_2SO_4		0.56	570 (280)	5.8	0.34

[a] Buffered solutions contain only the indicated buffer at $\mu = 0.5$ M. [b] Input power is at 632.8 nm. [c] Quantum yield for electron flow at $E^{\circ\prime}(H_2O/H_2)$. Data are ±15% and are uncorrected for reflection or solution absorption. [d] Photovoltages, as in Table III. [e] Defined in ref 8.

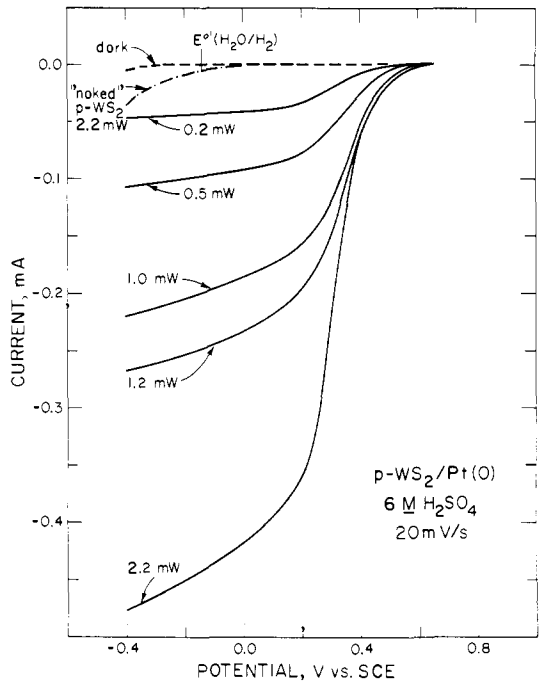

Figure 8. Steady-state photocurrent–voltage curves for a Pt-treated p-WS_2 electrode in 6 M H_2SO_4. $E^{\circ\prime}(H_2O/H_2)$ was measured at a Pt electrode. Irradiation was provided at 632.8 nm. Data from these curves are given in Table III.

electrolysis of H_2O and the input electrical power is diminished to the extent that illuminated p-WS_2 provides power. Note that η_{max} is a measure of the efficiency for the transduction of the optical input power to power needed to electrolyze H_2O. The η_{max} values in strong acid for H_2 generation are about the same as for the electricity generating systems based on the chemistry represented by eq 3 and 4. The evolution of H_2 from Pd- or Pt-treated WS_2 can be sustained at a significant current density and efficiency for prolonged periods. Figure 9 shows the photocurrent–time

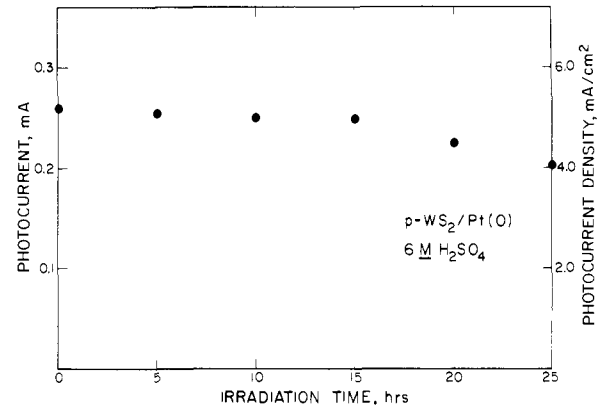

Figure 9. Plot of photocurrent against time for a ~0.05-cm² p-WS_2 electrode irradiated with 632.8-nm (~50 mW/cm²) light. The run was performed in deoxygenated 6 M H_2SO_4 with the photocathode held at +0.2 V vs. SCE.

profile for a Pt-treated WS_2 photocathode. Obviously, the current does decline somewhat during the ~25-h experiment, but it should be emphasized that there is no deliberately added Pt in the solution. The small amount of decline can be attributed to poisoning of the Pt. It has previously been noted that heavy metals can deposit onto the surface of the Pd catalyst to reduce the H_2 evolution current.[15a] Examination of Pd- or Pt-treated p-WS_2 photocathodes by XPS does show evidence for Hg but this could not always be correlated with a decline in photocurrent. The XPS does not show Pb, which could also be a possible catalyst poison.[15a] Generally, we have found far greater durablility from Pd- and Pt-treated p-WS_2 than from similarly treated p-Si[15b] or p-InP.[42] It is also noteworthy that high light intensity, up to ~70 mW/cm², Table III, does not lead to significant deterioration in H_2 evolution efficiency. This is in contrast to the situation found for the electricity-generating systems based on the one-electron redox couples. Presumably, the low concentrations used in those cases meant electron transfer was unable to compete effectively with recombination processes at high light intensities. In strong acid there is no significant depletion of H^+ activity at the light intensities used. However, as the acid strength is increased the $E^{\circ\prime}(H_2O/H_2)$ moves more positive giving a lower E_V(oc), accounting for a decline in η_{max} above 6 M H_2SO_4. Additional problems can be expected at the high H_2SO_4 concentration, since the solvent properties change significantly.

The final point with respect to the H_2 evolution is a strong decline in η_{max} as the pH is raised, Table IV. We attribute the decline in efficiency to the negative shift of $E^{\circ\prime}(H_2O/H_2)$ as the pH is raised, while E_{FB} is insensitive to pH, as shown by the pH independence of the E_V(oc) in the presence of $[MV]^{2+/+}$ or $[Fe(CN)_6]^{3-/4-}$. The low H^+ activity at higher pH's likely contributes to a lower rate of H_2 evolution. However, Pt electrodes give good current density for H_2 evolution with low overvoltage independent of the pH of the solutions used. This has been established by platinizing W surfaces with the same Pt coverage used for the p-WS_2. Thus, the main factor in lowering the efficiency of p-WS_2 for H_2 evolution at the high pH's seems to be the negative $E^{0\prime}(H_2O/H_2)$ resulting in consequences associated with junction breakdown, just as for $[MV]^{2+/+}$. The strong pH dependence on η_{max} for H_2 evolution substantiates the conclusions that the deposition of Pd or Pt onto p-WS_2 does not result in a Schottky barrier that would give a fixed efficiency. However, as noted above, the deposition of Pd or Pt onto p-WS_2 often leads to the undesirable formation of an ohmic contact that gives an electrode having very low or zero efficiency. To overcome the problems associated with the tendency to form an ohmic contact, we are currently pursuing the possibility of first coating the p-WS_2 surface with a redox polymer followed by deposition of the Pd

(42) Dominey, R. N.; Stalder, C.; Wrighton, M. S., to be submitted for publication.

or Pt onto the outermost surface as has been done with p-Si.[15a]

A final interesting point concerning p-WS_2 is that the photocurrent-voltage data for H_2 evolution in strong acid solution suggests that the photoelectrolysis of HBr according to eq 3 and 4 would be possible by using a cell employing a p-WS_2 photo-

$$2H^+ + 2e^- \rightarrow H_2 \text{ (at p-}WS_2\text{ photocathode)} \quad (3)$$

$$2Br^- + 2h^+ \rightarrow Br_2 \text{ (at n-}WS_2\text{ photoanode)} \quad (4)$$

cathode and an n-WS_2 photoanode. Indeed, the data[8] from Br^- photooxidation show that the n-WS_2 electrode gives its η_{max} at a potential where Pd-treated p-WS_2 gives its η_{max} for H_2 evolution, ~+0.3 V vs. SCE. Thus, visible illumination of the n-WS_2 shorted to the Pd-treated p-WS_2 should give good efficiency for the generation of Br_2 and H_2, respectively, from HBr. A similar double photoelectrode-based cell, p-InP/n-WSe_2, has recently been reported.[43] We find maximum initial efficiencies of >5% with 632.8 nm illumination at 20-40 mW/cm^2 are obtained under short-circuit conditions for a two compartment cell with aqueous 6 M H_2SO_4/2 M LiBr electrolyte in both compartments. Br_2, ~2 mM, was added to the photoanode compartment to poise the half-cell potential. Illumination intensities were adjusted until a small reduction in the intensity at either photoelectrode gave an equivalent decrease in full cell current. Unfortunately, while we have uncovered a situation where both the n- and p-type semiconductors should give optimum performance in the same medium, the WS_2 double photoelectrode-based cell for HBr electrolysis rapidly loses efficiency, owing to deterioration in performance of the photocathode. This result underscores the need to elaborate the conditions under which good performance for n- and p-type semiconductor electrodes can be simultaneously sustained.

Conclusions

Single-crystal p-type WS_2 photocathodes have a good wavelength response ($E_g \approx 1.3$ eV), a good output photovoltage (up to ~0.8 V), and are durable in a variety of solvent/electrolyte/redox couple combinations. Demonstrated overall efficiencies for the sustained conversion of 632.8-nm light to electricity exceeds 7%, and Pd- or Pt-treated p-WS_2-based cells evolve H_2 from acidic solutions with similar (~7%) efficiency at input visible light power densities of >50 mW/cm^2. The p-WS_2 is relatively free of surface states that would cause Fermi level pinning. A key point supporting this is that the dark oxidation of reduced species generally occurs positive of E_{FB} for couples having $E_{1/2}$ in a potential regime where the surface is not inverted. Over a wide range of E_{redox}, the p-WS_2 behaves ideally in that the photovoltage depends on E_{redox} in a manner consistent with a surface state-free interface. Sufficiently negative E_{redox} is associated with carrier inversion and, ultimately, junction breakdown of the WS_2/liquid interface. Good agreement is obtained between interfacial energetic measurements from cyclic voltammetry, interface capacitance, and steady-state photocurrent-voltage curves.

Acknowledgment. Work at M.I.T. was supported by GTE Laboratories, Inc., and by the U.S. Department of Energy, Office of Basic Energy Sciences, Division of Chemical Sciences. D.J.H. acknowledges support as an NSERC Fellow, 1980-present, and A.J.R. acknowledges support as an NPW Fellow, 1982-1983.

Registry No. WS_2, 12138-09-9; H_2, 1333-74-0; H_2O, 7732-18-5; Pd, 7440-05-3; Pt, 7440-06-4; $[MPT]^{+\cdot}$, 34510-35-5; MPT, 1207-72-3; $[TMPD]^{2+}$, 34527-56-5; $[TMPD]^{+\cdot}$, 34527-55-4; $[TTF]^{2+}$, 35079-57-3; $[TTF]^{+\cdot}$, 35079-56-2; $[Fe(\eta^5\text{-}C_6H_5)(\eta^5\text{-}C_5H_4CH_2N(CH_3)_3)]^{2+}$, 51150-57-3; $[Fe(\eta^5\text{-}C_6H_5)(\eta^5\text{-}C_5H_4CH_2N(CH_3)_3)]^{+}$, 33039-48-4; TTF, 31366-25-3; TCNE, 670-54-2; $[TCNE]^{-\cdot}$, 34512-48-6; TCNQ, 1518-16-7; $[TTNQ]^{-\cdot}$, 34507-61-4; $[TCNQ]^{2-}$, 48161-40-6; $[MV]^{2+}$, 4685-14-7; $[MV]^{+\cdot}$, 25239-55-8; $Ru(acac)_3$, 14284-93-6; $[Ru(acac)_3]^-$, 66560-52-9; MV, 25128-26-1; BAQ, 84-47-9; $[BAQ]^{-\cdot}$, 77898-33-0; $[BAQ]^{2-}$, 84878-05-7; $[IrCl_6]^{2-}$, 16918-91-5; $[IrCl_6]^{3-}$, 14648-50-1; $[Mo(CN)_8]^{3-}$, 17845-99-7; $[Mo(CN)_8]^{4-}$, 17923-49-8; $[Fe(CN)_6]^{3-}$, 13408-62-3; $[Fe(CN)_6]^{4-}$, 13408-63-4; $[Ru(NH_3)_6]^{3+}$, 18943-33-4; $[Ru(NH_3)_6]^{2+}$, 19052-44-9; $[Ru(NH_3)_6Cl_3]$, 14282-91-8; H_2SO_4, 7664-93-9; I_3^-, 14900-04-0; I^-, 20461-54-5; $[thianthrene]^{+\cdot}$, 34507-27-2; thianthrene, 92-85-3; [1,1'-diacetylferrocene]$^+$, 12277-02-0; 1,1'-diacetylferrocene, 1273-94-5; [acetylferrocene]$^+$, 32662-25-2; acetylferrocene, 1271-55-2; [ferrocene]$^+$, 12125-80-3; ferrocene, 102-54-5; chloranil, 118-75-2; $[chloranil]^{-\cdot}$, 17217-66-2; [decamethylferrocene]$^+$, 54182-41-1; decamethylferrocene, 12126-50-0; $[chloranil]^{2-}$, 55976-90-4; $[Ru(2,2'\text{-bipyridine})_3]^{2+}$, 15158-62-0; $[Ru(2,2'\text{-bipyridine})_3]^{+}$, 56977-24-3; $Ru(2,2'\text{-bipyridine})_3$, 74391-32-5; $[Ru(2,2'\text{-bipyridine})_3]^-$, 56977-23-2; KCl, 7447-40-7.

(43) Levy-Clement, C.; Heller, A.; Bonner, W. A.; Parkinson, B. A. *J. Electrochem. Soc.* **1982**, *129*, 1701.

Non-Koopmans' Theorem Effects in the He I Photoelectron Spectra of Polyenes

T. Koenig,* C. E. Klopfenstein, S. Southworth, J. A. Hoobler, R. A. Wielesek, T. Balle, W. Snell, and Daniel Imre

Contribution from the Department of Chemistry, University of Oregon, Eugene, Oregon 97403. *Received July 22, 1982*

Abstract: The predictions of the Koopmans' theorem MNDO model and the non-Koopmans' theorem (NKM) model for the photoelectron spectra of *p*-quinodimethane and its 2,5-dimethyl and perfluoro derivatives are discussed. The results of HAM/3-CI calculations support the NKM interpretation and indicate the weak feature at 13.4 eV in the PE spectrum of 1,1,4,4-tetrafluorobutadiene can be assigned to the lowest KTM "forbidden" transition in this case.

Dewar has recently[1] provided a critical discussion of our experimental results and of our interpretation of the He I photoelectron spectra of *p*-quinodimethane (**1**)[2] and its 2,5-dimethyl derivative (**2**).[3] In doing so he has provided an excellent focus on the question of the applicability of Koopmans' theorem[4] as an interpretive model (KTM) for the UV-PE spectra of such compounds. As Dewar points out, a distinction between the KTM

(1) Dewar, M. J. S. *J. Am. Chem. Soc.* **1982**, *104*, 1447.
(2) Koenig, T.; Wielesek, R. A.; Snell, W.; Balle, T. *J. Am. Chem. Soc.* **1975**, *97*, 3225.
(3) Koenig, T.; and Southworth, S. *J. Am. Chem. Soc.* **1977**, *99*, 2807.
(4) Koopmans, T. *Physica (Utrecht)* **1934**, *1*, 104.

0002-7863/83/1505-2256$01.50/0